

This document is the unedited Author's version of a Submitted Work that was subsequently accepted for publication in The Journal of Physical Chemistry C, copyright © American Chemical Society after peer review. To access the final edited and published work see <https://doi.org/10.1021/acs.jpcc.1c01550>

Access to this work was provided by the University of Maryland, Baltimore County (UMBC) ScholarWorks@UMBC digital repository on the Maryland Shared Open Access (MD-SOAR) platform.

**Please provide feedback**

Please support the ScholarWorks@UMBC repository by emailing [scholarworks-group@umbc.edu](mailto:scholarworks-group@umbc.edu) and telling us what having access to this work means to you and why it's important to you. Thank you.

# Positive and Negative Photoconductivity in Monolayer MoS<sub>2</sub> as a Function of Physisorbed Oxygen

Jon K. Gustafson\*, Daniel Wines, Ellen Gulian, Can Ataca\*, and L. Michael  
Hayden\*

Department of Physics, UMBC, 1000 Hilltop Circle, Baltimore, MD 21250, United States

\*Corresponding authors: [jgus1@umbc.edu](mailto:jgus1@umbc.edu), [ataca@umbc.edu](mailto:ataca@umbc.edu), [hayden@umbc.edu](mailto:hayden@umbc.edu)

## Abstract

We investigate the effect of molecular oxygen on the photoconductivity of monolayer MoS<sub>2</sub> via broad-band time-resolved terahertz spectroscopy. We observe that the photoconductivity of monolayer MoS<sub>2</sub> transitions from negative to positive when the environment of MoS<sub>2</sub> changes from vacuum to atmospheric pressure. We argue that this transition from negative to positive photoconductivity results from physically adsorbed oxygen depleting excess electrons from the *n*-type MoS<sub>2</sub>. We attribute the negative photoconductivity to negative trion formation, in which photoinduced excitons capture excess electrons from the MoS<sub>2</sub>. We attribute the positive photoconductivity to negative trion formation as well; however, in this case, photoinduced excitons capture photoinduced defect electrons rather than excess electrons, which have been immobilized by physisorbed oxygen. These results should prove useful to those who look to make sensors and other types of devices out of monolayer MoS<sub>2</sub> as physisorbed gases, particularly oxygen, can dramatically affect the conductivity of the monolayer.

## Introduction

Monolayer transition metal dichalcogenides (TMDs) are two-dimensional (2D) materials of the form  $\text{MX}_2$ , where M is a transition metal and X is a chalcogen atom. These materials have attracted much interest over the past several years because their unique electronic and optical properties make them suitable for a wide range of device applications.<sup>1,2</sup> Electrically, monolayer TMDs are direct-gap semiconductors with band gaps in the visible range.<sup>3</sup> They are therefore highly attractive for next generation field effect transistors (FETs).<sup>4</sup> Optically, monolayer TMDs are dominated by exciton and charged exciton (trion) complexes.<sup>5</sup> Due to spin-valley locking, these excitons and trions are valley dependent, thus making monolayer TMDs promising materials for quantum computing applications, particularly in the field of valleytronics.<sup>6-8</sup>

As researchers continue to look to make devices out of TMDs, it is clear that a complete understanding of how these materials behave is necessary, especially under real-world conditions where the TMDs will interact with external environments. Previous studies have shown that monolayer TMDs are extremely sensitive to molecular gases. Park et al.<sup>9</sup> and Qiu et al.<sup>10</sup> for example report that adsorbed  $\text{O}_2$  substantially reduces current in  $\text{MoS}_2$  FETs. Tongay et al.<sup>11, 12</sup> and Nan et al.<sup>13</sup> demonstrate that adsorbed gases, such as  $\text{O}_2$  and  $\text{N}_2$ , significantly enhance the photoluminescence of monolayer TMDs. Furthermore, Gogoi et al.<sup>14</sup> report that adsorbed  $\text{O}_2$  modulates the dielectric function of monolayer  $\text{MoS}_2$ . None of these studies however directly measured the effect of  $\text{O}_2$  on the photoconductivity of these 2D materials, which may be important for device realization.

We are primarily interested in understanding how  $\text{O}_2$  affects the photoconductivity of TMDs. To do so, we utilize time-resolved terahertz spectroscopy (TRTS). TRTS is an experimental technique that allows one to directly probe the photoconductivity of a material.

TRTS provides access to the frequency-dependent complex photoconductivity of a material, as well as insight into the dynamics of the photoconductivity with sub-picosecond resolution. A few groups have previously utilized TRTS to study the photoconductivity dynamics of TMDs;<sup>15-21</sup> however, in their work they have not addressed how O<sub>2</sub> modulates the photoconductivity response of TMDs.

In this paper, we study the effect of O<sub>2</sub> on the THz photoconductivity of chemical vapor deposition (CVD) grown monolayer MoS<sub>2</sub> via broad-band TRTS. We observe that the THz photoconductivity of monolayer MoS<sub>2</sub> changes from negative to positive as the environment of MoS<sub>2</sub> changes from vacuum to 760 Torr of O<sub>2</sub>. We attribute this behavior to physically adsorbed O<sub>2</sub> depleting excess electrons from the *n*-type MoS<sub>2</sub>. When the monolayer is exposed to vacuum, we observe negative photoconductivity, which we assign to negative trion formation, in which photogenerated excitons combine with excess electrons in the MoS<sub>2</sub>. These trions have reduced conductivity due to their increased effective mass. When the monolayer is exposed to oxygen, the O<sub>2</sub> physically adsorbs onto the surface of the MoS<sub>2</sub> and excess electrons transfer from the monolayer to the O<sub>2</sub>, which reduces the base conductivity of the MoS<sub>2</sub> significantly, to a nearly undoped state. With no base conductivity, the conductivity then increases upon photoexcitation. We assign this positive photoconductivity to defect-mediated negative trion formation, in which photoinduced excitons capture photoinduced defect electrons.

## **Experimental Section**

### Sample Preparation

Our monolayer MoS<sub>2</sub> sample was acquired commercially from 2D Semiconductors.<sup>22</sup> The sample was grown on a sapphire substrate via chemical vapor deposition and then later transferred to a TOPAS (cyclic olefin copolymer) substrate. The sample was slightly *n*-type.

## Time-Resolved Terahertz Spectroscopy

We utilized an optical-pump terahertz probe spectrometer to measure the photoconductivity of monolayer MoS<sub>2</sub>. Our TRTS setup is driven by a regeneratively amplified Ti:sapphire laser (Coherent Legend Elite Duo), which generates 30 fs pulses at a 1 kHz repetition rate with a central wavelength of 800 nm. The output of the laser system is split into two beams using a 50/50 beam splitter. One beam is used to pump an optical parametric amplifier (Coherent OperA Solo), which allows for tunable excitation pulses. The excitation beam diameter is roughly 2 mm. The other beam is then split again: one beam for terahertz generation and one for terahertz detection. Broad-band terahertz pulses are generated using a two-color, air-plasma technique,<sup>23</sup> where 800 nm light is focused through a BBO crystal and the fundamental and second harmonic are mixed in an air-plasma filament. Terahertz pulses are detected using electro-optic sampling<sup>24</sup> in a 300 μm thick GaP crystal, which provides continuous bandwidth from 0.5 to 8 THz.<sup>25, 26</sup> The terahertz beam diameter is roughly 800 μm at the sample. The entire beam path is purged with dry air in order to avoid water vapor absorption.

## **Results and Discussion**

In Figure 1, we present the ultraviolet-visible (UV-vis) absorption spectrum of our monolayer MoS<sub>2</sub> film at room temperature. Similar to others,<sup>16, 18</sup> we observe three resonances in the absorption spectrum, which correspond to the A, B, and C excitons. The A, B, and C excitons are located at 643 nm (1.93 eV), 600 nm (2.07 eV), and 429 nm (2.89 eV) respectively.

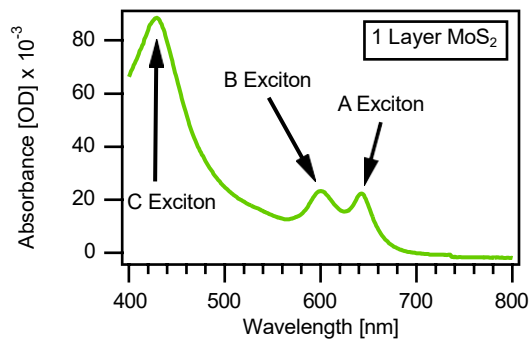


**Figure 1.** The ultraviolet-visible absorbance spectrum of monolayer MoS<sub>2</sub> on TOPAS (cyclic olefin copolymer) substrate at 300K. Peaks A, B, and C denote the different exciton resonances.

To probe the effect of O<sub>2</sub> on the photoinduced conductivity dynamics of our monolayer MoS<sub>2</sub> sample, we utilized TRTS. Here, we measured the fractional change in transmission of the peak of the terahertz waveform ( $\Delta E/E_t$ ) as a function of time after pump excitation when the MoS<sub>2</sub> was in vacuum and when the MoS<sub>2</sub> was in 760 Torr of O<sub>2</sub>. For both experiments, the MoS<sub>2</sub> was pumped on resonance with the A exciton at 300 K (643 nm). In vacuum (Figure 2a), we observed an ultrafast increase in  $\Delta E/E_t$  upon photoexcitation, indicating a photoinduced decrease in conductivity, since the photoconductivity,  $\Delta\sigma \sim -\Delta E/E_t$ . Following the decrease, the conductivity then recovered on a timescale on the order of several picoseconds. In the oxygen environment (Figure 2b), we observed an ultrafast decrease in  $\Delta E/E_t$  upon photoexcitation, indicating a photoinduced increase in conductivity. Following the increase, the conductivity then decayed rapidly within 1 ps to a nonzero level that persisted for over 200 picoseconds. In both the vacuum and oxygen MoS<sub>2</sub> photoconductivity dynamics, we observed a slight decrease in the photoconductivity of MoS<sub>2</sub>  $\sim 10.5$  ps after photoexcitation, which we attribute to a pump beam reflection off of the TOPAS substrate re-photoexciting the MoS<sub>2</sub>. We also observed that the switch between negative and positive photoconductivity is reversible.

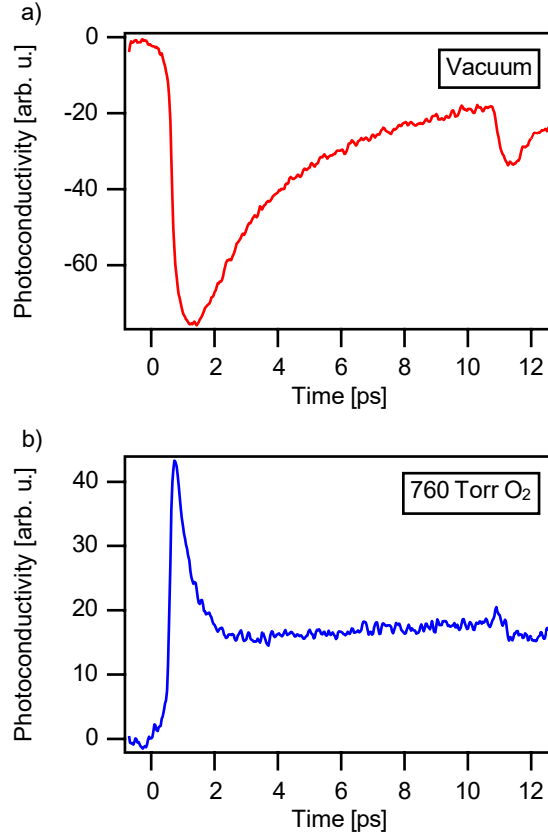


**Figure 2.** Terahertz photoconductivity  $\Delta\sigma \sim -\Delta E/E_1$  of monolayer MoS<sub>2</sub> in (a) vacuum and in (b) 760 Torr of O<sub>2</sub> as a function of time after pump excitation. The sample was photoexcited on resonance with the A exciton at 300 K (643 nm) with an incident fluence of  $\sim 4.5 \times 10^{14}$  photons/cm<sup>2</sup>.

To understand the photoinduced decrease in conductivity described in Figure 2a, we consider the role of doping in monolayer MoS<sub>2</sub>. Previous work reports that monolayer MoS<sub>2</sub> grown via chemical vapor deposition is *n*-type (has excess electrons).<sup>27</sup> Given that mobile electrons absorb THz radiation, we therefore expect our MoS<sub>2</sub> sample to have a base conductivity that is proportional to the excess electron concentration. Upon photoexcitation, we generate excitons in the MoS<sub>2</sub> since we photoexcite the sample with photons of the same energy as the A exciton. Therefore, immediately after photoexcitation, the MoS<sub>2</sub> has an exciton

population in addition to the excess electron population. Due to enhanced Columbic interactions, we expect the excess electrons to bind to the photogenerated excitons almost instantaneously<sup>15, 28</sup> to form negative trions. Trions, being three-body systems, have a higher effective mass than electrons and thus lower a mobility and conductivity. Since trions, which dominate the conductivity after photoexcitation, have lower conductivity than electrons, which dominate the conductivity before photoexcitation, the measured photoconductivity (the change in conductivity) of MoS<sub>2</sub> is negative. Lui et al. report negative photoconductivity in monolayer MoS<sub>2</sub> due to negative trion formation as well.<sup>15</sup>

To understand the photoinduced increase in conductivity described in Figure 2b, we consider the effect of oxygen on the MoS<sub>2</sub>. Previous work reports that when O<sub>2</sub> adsorbs onto the surface of MoS<sub>2</sub>, charge transfers from the MoS<sub>2</sub> to the O<sub>2</sub>.<sup>11, 12, 29-32</sup> We therefore expect the density of excess electrons in our *n*-type MoS<sub>2</sub> sample to decrease when oxygen is introduced to the environment of the MoS<sub>2</sub>. This depletion of excess charge consequently reduces the base conductivity of the MoS<sub>2</sub>, nearly to an un-doped level, depending on the oxygen coverage and original doping level. Upon on-resonance photoexcitation, we generate a population of excitons; however, unlike before when the MoS<sub>2</sub> was in vacuum, we do not have a population of excess electrons for the excitons to form negative trions with because of the O<sub>2</sub> adsorption. Furthermore, excitons themselves do not contribute strongly to the THz conductivity since they are charge neutral and have binding energies outside of our experimental window. To understand the increase in conductivity, we also consider the role defects play in the system. In CVD-grown monolayer MoS<sub>2</sub>, sulfur vacancies, the most prominent type of defect,<sup>33, 34</sup> introduce states within the band gap.<sup>35</sup> The energy supplied by the on-resonance pump beam can promote electrons trapped in these defect states to the conduction band. These photoinduced defect

electrons can then bind to the photogenerated excitons to form negative trions. Since the base conductivity of the MoS<sub>2</sub> is reduced due to O<sub>2</sub> adsorption, the conductivity after photoexcitation, which is determined by the negative trions, is greater than the conductivity before photoexcitation. The measured photoconductivity (change in conductivity) of MoS<sub>2</sub> is therefore positive.

We attribute the decay of the negative and positive photoconductivity to defects. This is because trions decay predominately through defect-mediated processes.<sup>15, 20</sup> In this decay mechanism, trions become trapped in defect states that are located in the band gap and thus no longer contribute to the conductivity. The picosecond timescale decay we observe in the negative photoconductivity and the sub-picosecond timescale decay we observe in the positive photoconductivity supports this defect-mediated decay mechanism. When the photoconductivity is positive, trion formation is defect mediated. Electrons are promoted from defect states to the conduction band so that they can then bind to photogenerated excitons to form trions. Defect states are now unoccupied and can thus trap trions. When the photoconductivity is negative, trions form when excess electrons in the conduction band bind to photogenerated excitons. This process is not defect mediated; however, defects still play a role in the photoconductivity in the sense that the excitation pulse promotes electrons in defect states to the conduction band, which leaves defect states unoccupied to trap trions. Since the conduction band is initially occupied though with excess electrons, fewer defect electrons can be photoexcited than when the photoconductivity is positive, in which the conduction band is unoccupied. Since there are fewer states available to trap trions, the negative photoconductivity should decay slower than the positive photoconductivity, which is what we observe.

We attribute the long-lived photoconductivity observed when monolayer MoS<sub>2</sub> is in oxygen to photoinduced oxygen desorption. From kinetic theory, it is known that as temperature increases, the rate of O<sub>2</sub> desorption increases. In our TRTS experiments, the excitation pulse increases the temperature of the MoS<sub>2</sub> (see Supporting Information for a discussion on the laser heating effect). Therefore, upon photoexcitation, we expect some of the O<sub>2</sub> to desorb from the surface of the MoS<sub>2</sub>. As these O<sub>2</sub> molecules desorb, depleted electrons transfer back to the MoS<sub>2</sub> and therefore increase the MoS<sub>2</sub> conductivity. Since there are no holes for these electrons to relax to (because these electrons were not photoexcited from the valence band), the photoconductivity persists. From 2 to 10 ps after photoexcitation, the photoconductivity actually rises slightly instead of decaying because oxygen is still desorbing from the surface. The decrease in the photoconductivity we observe at around 10.5 ps after photoexcitation supports this idea that electrons dominate the long-lived photoconductivity, through the following argument. As mentioned earlier, the decrease in the photoconductivity at around 10.5 ps after photoexcitation occurs because a pump beam reflection off of the TOPAS substrate re-photoexcites the MoS<sub>2</sub>. We know from previous discussion that MoS<sub>2</sub> exhibits a photoinduced decrease in conductivity when MoS<sub>2</sub> is *n*-type. Since the pump reflection causes a photoinduced decrease in the conductivity, the MoS<sub>2</sub> at the time of the reflection must then be *n*-type, which suggests that electrons determine the long-lived photoconductivity.

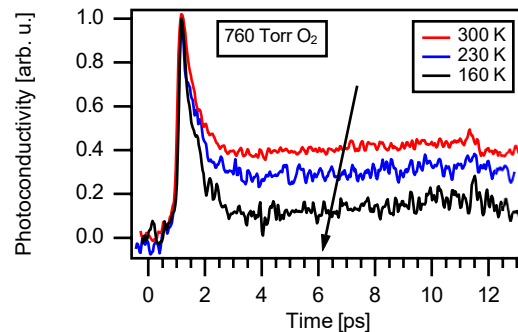


**Figure 3.** The terahertz photoconductivity of monolayer MoS<sub>2</sub> as a function of time after photoexcitation at 300 K (red trace), 230 K (blue trace), and 160 K (black trace). The sample was pumped on resonance with the A exciton (643 nm at 300 K, 626 nm at 230 K, and 616 nm at 160 K) with an incident fluence of  $\sim 4.5 \times 10^{14}$  photons/cm<sup>2</sup>.

We also looked at the effect of temperature on the long-lived photoconductivity of monolayer MoS<sub>2</sub> in oxygen. In Figure 3, we present the photoconductivity dynamics of monolayer MoS<sub>2</sub> in 760 Torr of O<sub>2</sub> at 300 K, 230 K, and 160 K normalized to their respective peaks. At all three temperatures, we excited the MoS<sub>2</sub> on resonance with the A exciton (see Supporting Information for the A exciton's temperature dependence). From these measurements, we find that the long-lived photoconductivity decreases as the temperature decreases. This behavior supports the photoinduced oxygen desorption mechanism described above. As the temperature decreases, fewer oxygen molecules desorb from the surface of the MoS<sub>2</sub> upon photoexcitation and thus, fewer electrons transfer back to the MoS<sub>2</sub>. With fewer electrons in the MoS<sub>2</sub>, the long-lived photoconductivity, which is due to these electrons, then decreases.

To further investigate the effect of O<sub>2</sub> on the photoconductivity of monolayer MoS<sub>2</sub>, we extracted the complex frequency-dependent sheet photoconductivity by recording the entire fractional pump-induced modulation of the terahertz waveform (Figures 4a and 4c) using our TRTS spectrometer (see the Supporting Information for details on calculating the complex sheet photoconductivity). In Figure 4b, we present the sheet photoconductivity of monolayer MoS<sub>2</sub> in vacuum at 1 ps after photoexcitation. In Figure 4d, we present the sheet photoconductivity of monolayer MoS<sub>2</sub> in oxygen at 500 fs after photoexcitation. We excited the MoS<sub>2</sub> on resonance with the A exciton at 300K for both of these sheet photoconductivity measurements. In vacuum, we find that both the real and imaginary parts of the photoconductivity are negative. In the

oxygen environment, we find that the real part of the photoconductivity is positive, and the imaginary part of the photoconductivity is negative. In an effort to understand these frequency-dependent photoconductivity curves, we employ a multi-component model (see Supporting Information).

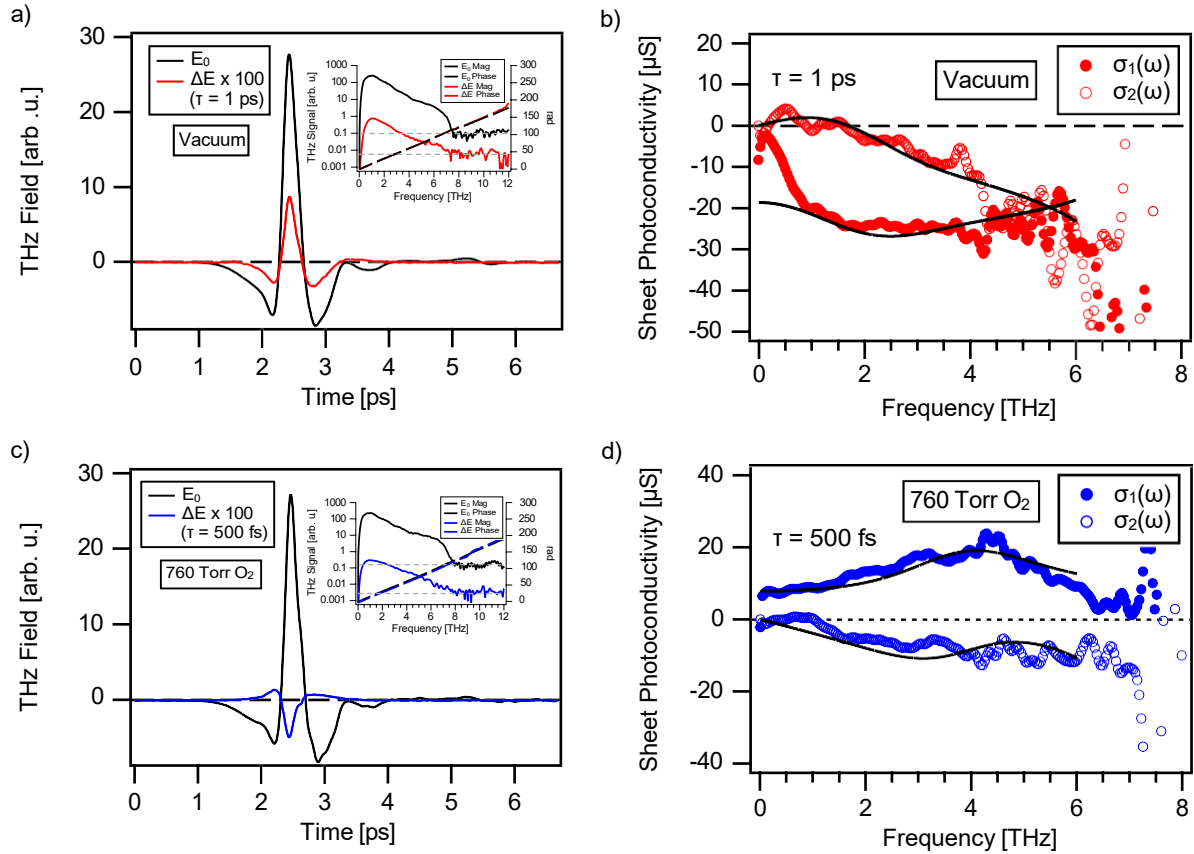


**Figure 4.** The THz waveform  $E_1(t)$  (black traces) and the pump-induced modulation of the THz waveform  $\Delta E(t)$  of monolayer MoS<sub>2</sub> in (a) vacuum (red trace) and in (c) 760 Torr of O<sub>2</sub> (blue trace). Insets plot the Fourier transforms of  $E_1(t)$  and  $\Delta E(t)$  (solid (dashed) lines are the magnitudes (phases) of the transforms and dotted gray lines are the noise floors for the respective spectra). The complex frequency-dependent sheet photoconductivity of monolayer MoS<sub>2</sub> in (b) vacuum and in (d) 760 Torr of O<sub>2</sub> at 1 ps and 500 fs after photoexcitation respectively. The MoS<sub>2</sub> was pumped on resonance with the A exciton at 300 K (643 nm). The absorbed fluence was  $\sim 2.4$

$\times 10^{13}$  photons/cm<sup>2</sup>. Solid (open) circles are the real (imaginary) part of the induced photoconductivity. The solid lines over the circles represent fits to the photoconductivity.

For MoS<sub>2</sub> in vacuum, we know from previous discussion that the conductivity after photoexcitation is attributed to negative trions and that the conductivity before photoexcitation is attributed to excess electrons. Therefore, we model the sheet photoconductivity as  $\Delta\sigma = \sigma'' - \sigma_{\#}$ , where  $\sigma''$  is the conductivity due to the trions and  $\sigma_{\#}$  is the conductivity due to the excess electrons. Our previous work<sup>20</sup> showed that trions in TMDs contribute to the conductivity in three ways: a Drude response, a broad resonance response due to charge buildup at grain boundaries, and a dissociation response at the trion binding energy. For the trion component  $\sigma''$ , we model the conductivity with these three responses. For the electron component  $\sigma_{\#}$ , we model the conductivity with only a Drude response and a broad resonance response. In the Supporting Information, we provide more details on this fit function, as well as a table with the resulting fit parameters. In Figure 4b, we plot the fit to the real and imaginary parts of the sheet photoconductivity (black traces). We find that our model agrees very well with the data, thus further confirming that the negative photoconductivity of monolayer MoS<sub>2</sub> in vacuum is due to the negative trion formation mechanism described earlier.

For MoS<sub>2</sub> in oxygen (Figure 4d), we know from previous discussion that the conductivity after photoexcitation is due to negative trions and that the conductivity before photoexcitation is negligible since oxygen adsorption depletes excess electrons from the MoS<sub>2</sub>. We therefore model the sheet photoconductivity with just a trion component,  $\Delta\sigma = \sigma''$ . Here  $\sigma''$  has a Drude response, a broad resonance response, and a dissociation response. In the Supporting Information, we provide the fitting function, as well as a table with the resulting fit parameters. In Figure 4d, we

plot the fit to the real and imaginary parts of the sheet photoconductivity (black traces). We again find that the fit models the data very well, which further verifies that the positive photoconductivity of monolayer MoS<sub>2</sub> in oxygen is a consequence of oxygen adsorption depleting excess electrons from the MoS<sub>2</sub>. The resulting fit also confirms the defect-mediated nature of trion formation that occurs when MoS<sub>2</sub> is in an oxygen environment. From Table S2, we find that the total trion concentration is roughly half of the absorbed fluence. In the defect mediated trion formation mechanism discussed earlier, a trion forms when an electron is photoexcited from a defect state located in the band gap to the conduction band and then binds to a photogenerated exciton. Two photons are required to form one trion (one to promote an electron to the conduction band and one to create an exciton). Therefore, the total trion concentration should be one-half of the absorbed fluence.

To better understand the charge transfer process between MoS<sub>2</sub> and adsorbed O<sub>2</sub>, we simulated the interaction between monolayer MoS<sub>2</sub> and O<sub>2</sub> using density functional theory (DFT) and *ab initio* molecular dynamics (MD). From these calculations, we find that up to 0.2 electrons per O<sub>2</sub> molecule can transfer from the MoS<sub>2</sub> to the physically adsorbed oxygen (See Supporting Information for more details). We then applied a Langmuir adsorption model to estimate the amount of oxygen adsorbed on the surface of the MoS<sub>2</sub>. For steady-state physical adsorption, the fraction of adsorption sites occupied by O<sub>2</sub> molecules,  $\theta$ , is given by

$$\theta = \frac{1}{1 + \frac{u_{\text{attempt}} N}{F} e^{-\frac{E_{\text{desorption}} + E_{\text{activation}}}{kT}}} \quad (1)$$

where  $u_{\text{attempt}}$  is the attempt frequency,  $N$  is the density of adsorption sites,  $F$  is the gas impingement flux,  $E_{\text{desorption}}$  is the desorption energy,  $E_{\text{activation}}$  is the activation energy,  $k$  is Boltzmann's constant, and  $T$  is temperature. The attempt frequency is given by  $u_{\text{attempt}} = kT/h$ , where  $h$  is

Planck's constant. The gas impingement flux is represented by  $F = P/\sqrt{2\pi mkT}$ , where  $P$  is the gas pressure and  $m$  is the molecular mass. Setting  $P = 760$  Torr,  $T = 300$  K,  $E_+ = 0$  meV,  $E_{\#} = 126$  meV,  $m = 5.31 \times 10^{-26}$  kg, and  $N = 7.1 \times 10^{17}$  cm<sup>-2</sup> (corresponding to one site per  $4 \times 4$  supercell), we calculate that  $\theta = 0.076$  and therefore estimate the amount of oxygen adsorbed on our sample, given by  $\theta \times N$ , to be roughly  $5.3 \times 10^{17}$  cm<sup>-2</sup>. Given this oxygen coverage of  $\sim 5.3 \times 10^{17}$  cm<sup>-2</sup> and knowing that 0.2 electrons transfer per O<sub>2</sub> molecule, we then calculate the total charge transfer. By multiplying  $5.3 \times 10^{17}$  cm<sup>-2</sup> and 0.2 electrons per O<sub>2</sub>, we estimate the concentration of electrons that transfer from the MoS<sub>2</sub> to the oxygen to be approximately  $1.1 \times 10^{17}$  cm<sup>-2</sup>. This value of  $1.1 \times 10^{17}$  cm<sup>-2</sup> is comparable to the estimated doping level of our *n*-type MoS<sub>2</sub> sample,  $3.1 \times 10^{17}$  cm<sup>-2</sup>, which indicates that the adsorbed O<sub>2</sub> significantly depletes electrons from our MoS<sub>2</sub> sample. This significant depletion explains why we experimentally observe a dramatic change in the photoconductivity (from negative to positive) upon introducing 760 Torr of O<sub>2</sub> to our sample.

At lower oxygen pressures, we calculate that there is insufficient O<sub>2</sub> coverage to deplete all of the electrons from the MoS<sub>2</sub>. To investigate the photoconductivity at this reduced doping state (exhibited at low O<sub>2</sub> pressures), we measured the THz photoconductivity dynamics as we pulled a vacuum on the sample (shown in Figure 5). In Figure 5, we observe that the photoconductivity has both a positive and negative component. Furthermore, we find that as we pull a vacuum (O<sub>2</sub> coverage decreases), the positive photoconductivity decreases while the magnitude of the negative photoconductivity increases. This behavior is a consequence of the competition between defect-mediated trion formation (responsible for the positive photoconductivity) and trion formation due to photogenerated excitons capturing excess charge from the monolayer (responsible for the negative photoconductivity).

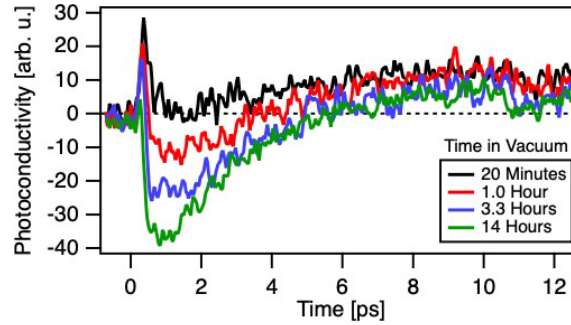


**Figure 5.** Terahertz photoconductivity dynamics of monolayer MoS<sub>2</sub> after 20 minutes in vacuum (black trace), 1 hour in vacuum (red trace), 3.3 hours in vacuum (blue trace), and 14 hours in vacuum (green trace). The MoS<sub>2</sub> was pumped on resonance with the A exciton at 300 K (643 nm) with an incident fluence of  $\sim 4.5 \times 10^{10}$  cm<sup>-2</sup>.

## Conclusions

In summary, we have shown using broad-band TRTS that when the environment of monolayer MoS<sub>2</sub> changes from vacuum to 760 Torr of O<sub>2</sub>, the photoconductivity changes from negative to positive. We find that this behavior is a consequence of physically adsorbed O<sub>2</sub> depleting excess electrons from the *n*-type MoS<sub>2</sub>. In vacuum, excess electrons bind to photogenerated excitons to form negative trions that have reduced conductivity. In oxygen, photoexcited defect electrons bind to photogenerated excitons to form negative trions that increase the conductivity. Further analysis shows that photoinduced O<sub>2</sub> desorption creates a long-lived conductivity in MoS<sub>2</sub> that is dominated by electrons that transfer back to the MoS<sub>2</sub>. This long-lived photoconductivity component does not occur when MoS<sub>2</sub> is in vacuum since no oxygen is present before photoexcitation. These results and analysis provide valuable insight into the effect of O<sub>2</sub> on the photoconductivity of MoS<sub>2</sub> and therefore should be useful to those who look to make devices out of MoS<sub>2</sub> and point to the need to potentially passivate the effects of adsorbed gases on TMD monolayers.

## Supporting Information

A discussion on laser heating, details concerning the measurement of the temperature-dependent absorption spectrum, details on the calculation of the photoconductivity, a discussion on fitting the photoconductivity, details about the computational methods, adsorption and charge transfer calculations, molecular dynamics results, density of states calculations, and charge density difference calculations at different coverages.

## Acknowledgments

J.K.G. and L.M.H. acknowledge support from a UMBC START grant. J.K.G. also acknowledges the support of the Department of Education through a GAANN Fellowship under award number P200A150003-17. E.G. acknowledges support from a UMBC URA Scholarship. D.W. and C.A. acknowledge support by the National Science Foundation through the Division of Materials Research under NSF DMR-1726213 Grant.

## References

1. Xia, F. N.; Wang, H.; Xiao, D.; Dubey, M.; Ramasubramaniam, A., Two-Dimensional Material Nanophotonics. *Nature Photonics* **2014**, *8*, 899-907.
2. Mak, K. F.; Shan, J., Photonics and Optoelectronics of 2D Semiconductor Transition Metal Dichalcogenides. *Nature Photonics* **2016**, *10*, 216-226.
3. Yun, W. S.; Han, S. W.; Hong, S. C.; Kim, I. G.; Lee, J. D., Thickness and Strain Effects on Electronic Structures of Transition Metal Dichalcogenides: 2H-MX<sub>2</sub> Semiconductors (M = Mo, W; X = S, Se, Te). *Physical Review B* **2012**, *85*, 033305.
4. Radisavljevic, B.; Radenovic, A.; Brivio, J.; Giacometti, V.; Kis, A., Single-Layer MoS<sub>2</sub> Transistors. *Nature Nanotechnology* **2011**, *6*, 147-150.
5. Wang, G.; Chernikov, A.; Glazov, M. M.; Heinz, T. F.; Marie, X.; Amand, T.; Urbaszek, B., Colloquium: Excitons in Atomically Thin Transition Metal Dichalcogenides. *Reviews of Modern Physics* **2018**, *90*, 021001.
6. Liu, Y. P.; Gao, Y. J.; Zhang, S. Y.; He, J.; Yu, J.; Liu, Z. W., Valleytronics in Transition Metal Dichalcogenides Materials. *Nano Research* **2019**, *12*, 2695-2711.
7. Xiao, D.; Liu, G. B.; Feng, W. X.; Xu, X. D.; Yao, W., Coupled Spin and Valley Physics in Monolayers of MoS<sub>2</sub> and Other Group-VI Dichalcogenides. *Physical Review Letters* **2012**, *108*, 196802.

8. Mak, K. F.; He, K. L.; Shan, J.; Heinz, T. F., Control of Valley Polarization in Monolayer MoS<sub>2</sub> by Optical Helicity. *Nature Nanotechnology* **2012**, *7*, 494-498.
9. Park, W.; Park, J.; Jang, J.; Lee, H.; Jeong, H.; Cho, K.; Hong, S.; Lee, T., Oxygen Environmental and Passivation Effects on Molybdenum Disulfide Field Effect Transistors. *Nanotechnology* **2013**, *24*, 095202.
10. Qiu, H.; Pan, L.; Yao, Z.; Li, J.; Shi, Y.; Wang, X., Electrical Characterization of Back-Gated Bi-Layer MoS<sub>2</sub> Field-Effect Transistors and the Effect of Ambient on Their Performances. *Applied Physics Letters* **2012**, *100*, 123104.
11. Tongay, S.; Zhou, J.; Ataca, C.; Liu, J.; Kang, J. S.; Matthews, T. S.; You, L.; Li, J.; Grossman, J. C.; Wu, J., Broad-Range Modulation of Light Emission in Two-Dimensional Semiconductors by Molecular Physisorption Gating. *Nano Letters* **2013**, *13*, 2831-2836.
12. Tongay, S.; Suh, J.; Ataca, C.; Fan, W.; Luce, A.; Kang, J. S.; Liu, J.; Ko, C.; Raghunathan, R.; Zhou, J.; Ogletree, F.; Li, J. B.; Grossman, J. C.; Wu, J., Defects Activated Photoluminescence in Two-Dimensional Semiconductors: Interplay Between Bound, Charged, and Free Excitons. *Scientific Reports* **2013**, *3*, 2657.
13. Nan, H. Y.; Wang, Z. L.; Wang, W. H.; Liang, Z.; Lu, Y.; Chen, Q.; He, D. W.; Tan, P. H.; Miao, F.; Wang, X. R.; Wang, J. L.; Ni, Z. H., Strong Photoluminescence Enhancement of MoS<sub>2</sub> through Defect Engineering and Oxygen Bonding. *ACS Nano* **2014**, *8*, 5738-5745.
14. Gogoi, P. K.; Hu, Z. L.; Wang, Q. X.; Carvalho, A.; Schmidt, D.; Yin, X. M.; Chang, Y. H.; Li, L. J.; Sow, C. H.; Neto, A. H. C.; Breese, M. B. H.; Rusydi, A.; Wee, A. T. S., Oxygen Passivation Mediated Tunability of Trion and Excitons in MoS<sub>2</sub>. *Physical Review Letters* **2017**, *119*, 077402.
15. Lui, C. H.; Frenzel, A. J.; Pilon, D. V.; Lee, Y.-H.; Ling, X.; Akselrod, G. M.; Kong, J.; Gedik, N., Trion-Induced Negative Photoconductivity in Monolayer MoS<sub>2</sub>. *Physical Review Letters* **2014**, *113*, 166801.
16. Docherty, C. J.; Parkinson, P.; Joyce, H. J.; Chiu, M.; Chen, C.; Lee, M.; Li, L.; Herz, L. M.; Johnston, M. B., Ultrafast Transient Terahertz Conductivity of Monolayer MoS<sub>2</sub> and WSe<sub>2</sub> Grown by Chemical Vapor Deposition. *ACS Nano* **2014**, *8*, 11147-11153.
17. Kar, S.; Su, Y.; Nair, R. R.; Sood, A. K., Probing Photoexcited Carriers in a Few-Layer MoS<sub>2</sub> Laminate by Time-Resolved Optical Pump-Terahertz Probe Spectroscopy. *ACS Nano* **2015**, *9*, 12004-12010.
18. Cunningham, P. D.; McCreary, K. M.; Hanbicki, A. T.; Currie, M.; Jonker, B. T.; Hayden, L. M., Charge Trapping and Exciton Dynamics in Large-Area CVD Grown MoS<sub>2</sub>. *Journal of Physical Chemistry C* **2016**, *120*, 5819-5826.
19. Xing, X.; Zhao, L. T.; Zhang, Z. Y.; Liu, X. K.; Zhang, K. L.; Yu, Y.; Lin, X.; Chen, H. Y.; Chen, J. Q.; Jin, Z. M.; Xu, J. H.; Ma, G. H., Role of Photoinduced Exciton in the Transient Terahertz Conductivity of Few-Layer WS<sub>2</sub> Laminate. *Journal of Physical Chemistry C* **2017**, *121*, 20451-20457.
20. Gustafson, J. K.; Cunningham, P. D.; McCreary, K. M.; Jonker, B. T.; Hayden, L. M., Ultrafast Carrier Dynamics of Monolayer WS<sub>2</sub> via Broad-Band Time-Resolved Terahertz Spectroscopy. *Journal of Physical Chemistry C* **2019**, *123*, 30676-30683.
21. Liu, X. F.; Yu, H. Y.; Ji, Q. Q.; Gao, Z. H.; Ge, S. F.; Qiu, J.; Liu, Z. F.; Zhang, Y. F.; Sun, D., An Ultrafast Terahertz Probe of the Transient Evolution of the Charged and Neutral Phase of Photo-Excited Electron-Hole Gas in a Monolayer Semiconductor. *2D Materials* **2016**, *3*, 014001.

22. 2D Semiconductor CVD MoS<sub>2</sub> Monolayers. <https://www.2dsemiconductors.com/full-area-coverage-monolayer-mos2-on-c-cut-sapphire/> (accessed April 1, 2021).
23. Xie, X.; Dai, J. M.; Zhang, X. C., Coherent Control of THz Wave Generation in Ambient Air. *Physical Review Letters* **2006**, *96*, 075005.
24. Planken, P. C. M.; Nienhuys, H. K.; Bakker, H. J.; Wenckebach, T., Measurement and Calculation of the Orientation Dependence of Terahertz Pulse Detection in ZnTe. *Journal of the Optical Society of America B-Optical Physics* **2001**, *18*, 313-317.
25. Wu, Q.; Zhang, X. C., 7 Terahertz Broadband GaP Electro-Optic Sensor. *Applied Physics Letters* **1997**, *70*, 1784-1786.
26. Chakkittakandy, R.; Corver, J.; Planken, P. C. M., Quasi-Near Field Terahertz Generation and Detection. *Optics Express* **2008**, *16*, 12794-12805.
27. Lee, Y. H.; Zhang, X. Q.; Zhang, W. J.; Chang, M. T.; Lin, C. T.; Chang, K. D.; Yu, Y. C.; Wang, J. T. W.; Chang, C. S.; Li, L. J.; Lin, T. W., Synthesis of Large-Area MoS<sub>2</sub> Atomic Layers with Chemical Vapor Deposition. *Advanced Materials* **2012**, *24*, 2320-2325.
28. Steinleitner, P.; Merkl, P.; Nagler, P.; Mornhinweg, J.; Schuller, C.; Korn, T.; Chernikov, A.; Huber, R., Direct Observation of Ultrafast Exciton Formation in a Monolayer of WSe<sub>2</sub>. *Nano Letters* **2017**, *17*, 1455-1460.
29. Liu, H.; Han, N.; Zhao, J., Atomistic Insight into the Oxidation of Monolayer Transition Metal Dichalcogenides: From Structures to Electronic Properties. *Rsc Advances* **2015**, *5*, 17572-17581.
30. Liu, Y.; Stradins, P.; Wei, S., Air Passivation of Chalcogen Vacancies in Two-Dimensional Semiconductors. *Angewandte Chemie-International Edition* **2016**, *55*, 965-968.
31. Yue, Q.; Shao, Z.; Chang, S.; Li, J., Adsorption of Gas Molecules on Monolayer MoS<sub>2</sub> and Effect of Applied Electric Field. *Nanoscale Research Letters* **2013**, *8*, 425.
32. Qi, L.; Wang, Y.; Shen, L.; Wu, Y. H., Chemisorption-Induced n-Doping of MoS<sub>2</sub> by Oxygen. *Applied Physics Letters* **2016**, *108* (6).
33. Hong, J. H.; Hu, Z. X.; Probert, M.; Li, K.; Lv, D. H.; Yang, X. N.; Gu, L.; Mao, N. N.; Feng, Q. L.; Xie, L. M.; Zhang, J.; Wu, D. Z.; Zhang, Z. Y.; Jin, C. H.; Ji, W.; Zhang, X. X.; Yuan, J.; Zhang, Z., Exploring Atomic Defects in Molybdenum Disulphide Monolayers. *Nature Communications* **2015**, *6*, 6293.
34. Qiu, H.; Xu, T.; Wang, Z. L.; Ren, W.; Nan, H. Y.; Ni, Z. H.; Chen, Q.; Yuan, S. J.; Miao, F.; Song, F. Q.; Long, G.; Shi, Y.; Sun, L. T.; Wang, J. L.; Wang, X. R., Hopping Transport Through Defect-Induced Localized States in Molybdenum Disulphide. *Nature Communications* **2013**, *4*, 2642.
35. Salehi, S.; Saffarzadeh, A., Optoelectronic Properties of Defective MoS<sub>2</sub> and WS<sub>2</sub> Monolayers. *Journal of Physics and Chemistry of Solids* **2018**, *121*, 172-176.

## TOC Graphic

